# $4\pi$ Compton Imaging Using a 3-D Position-Sensitive CdZnTe Detector Via Weighted List-Mode Maximum Likelihood

Carolyn E. Lehner, *Student Member, IEEE*, Zhong He, *Senior Member, IEEE*, and Feng Zhang, *Student Member, IEEE*

***Abstract*—In this paper, we describe a $4\pi$ Compton imager composed of a single $15\ \mathrm{mm} \times 15\ \mathrm{mm} \times 10\ \mathrm{mm}$ CdZnTe detector. Full $4\pi$ images are reconstructed via list-mode maximum likelihood (ML). A new weighting method for ML reconstruction is proposed in which the contributions of small-uncertainty sequences are enhanced relative to sequences with large uncertainties. The new reconstruction method is compared with traditional ML techniques for measured imaging data. The $4\pi$ Compton imager has a measured intrinsic imaging efficiency of nearly 2% and an imaging resolution using the weighted ML reconstruction method of 17° at 662 keV after 10 iterations.**

***Index Terms*—Cadmium zinc telluride, Compton camera, gamma-ray imaging, gamma-ray tracking, image reconstruction, maximum likelihood estimation.**

## I. Introduction

TRADITIONALLY, Compton imaging has been performed with two detectors or arrays of detectors. Sequences in which the gamma ray scatters in the front plane detector and is absorbed in the back plane detector generate a cone of possible source locations. Overlapping cones projected onto the source plane from multiple sequences yield an image of the source distribution. Compton imaging performed in this manner suffers from several disadvantages compared to other imaging modalities for energies below 1 MeV. First, the efficiency of the imagers is typically low due to the separation distance between the detectors and the limited solid angle subtended by the back plane detector. Also, the second detector must be physically shielded from direct irradiation, increasing size and weight and limiting the field-of-view of the instrument.

With a single-detector imager the back plane shielding can be eliminated. In addition, the efficiency can increase by 1–2 orders of magnitude because there is no separation between detectors. Kroeger, *et al.*, [1] have shown the ability to resolve a 511-keV source from a 662-keV source separated by about 15° using a single planar Ge strip detector. Schmid *et al.*, [2] have attempted operating a large volume tapered segmented Ge detector (GRETA) as a Compton imager.

Manuscript received November 14, 2003; revised May 13, 2004. This work was supported by the U.S. Department of Energy Office NA-22 and was performed in part under appointment to the U.S. Department of Energy's Nuclear Engineering and Health Physics Fellowship sponsored by the U.S. Department of Energy Office of Nuclear Energy, Science, and Technology.

The authors are with the University of Michigan, Ann Arbor, MI 48109 USA (e-mail: clehner@umich.edu; hezhong@umich.edu; zhangf@umich.edu).

Digital Object Identifier 10.1109/TNS.2004.832573

In this paper, we describe a Compton imager composed of a single $15\ \mathrm{mm} \times 15\ \mathrm{mm} \times 10\ \mathrm{mm}$ CdZnTe detector. The anode is pixellated into an $11 \times 11$ array as in [3] to provide position sensitivity in two dimensions. The third coordinate is determined from the observed timing of signals in the detector. The position resolution is approximately 1.2 mm in the lateral dimensions and 1 mm in depth. Energy resolution for single- and double-pixel events is 1.3% and 2%, respectively, at 662 keV.

Backprojection filtering and maximum likelihood estimation via the expectation maximum algorithm (MLEM) [4] are the most common reconstruction techniques for Compton imaging. We implemented list-mode MLEM as in [5] to reconstruct $4\pi$ images. Furthermore, we introduce a new weighting method for list-mode MLEM based on estimated angular uncertainties. In this paper, we demonstrate improved imaging capabilities in $4\pi$ using weighted MLEM compared with traditional list-mode MLEM.

## II. $4\pi$ Compton Imaging

The method of Compton imaging is well known. Once the sequence of events is determined, the initial scatter angle $\theta$ is calculated using the Compton scatter formula, derived under the conditions that the electron is unbound and at rest

$$\cos\theta = 1 - \frac{m_e c^2 E_1}{E_0(E_0 - E_1)} \tag{1}$$

where $m_e c^2$ is the rest mass energy of an electron, $E_1$ is the energy deposited in the first interaction, and $E_0$ is the initial gamma-ray energy (calculated here by summing the observed deposited energies). Then it is possible to generate a backprojection cone with an opening angle $\theta$ and an axis defined by the ray from the second to the first interaction point. The sum of cones over many gamma-ray sequences yields the source position. Typically, this summation is performed in the source plane, and a planar image with limited field-of-view is generated.

Full $4\pi$ imaging can be achieved with a single detector because there is no preference for gamma rays incident from a particular direction, unlike Compton imagers composed of two detectors. Instead of reconstructing a planar image, the image is reconstructed on the surface of a sphere surrounding the detector as in Fig. 1. In the far-field approximation—the distance from the source to the detector is much larger than the distance from any point in the detector to the center of the detector—it

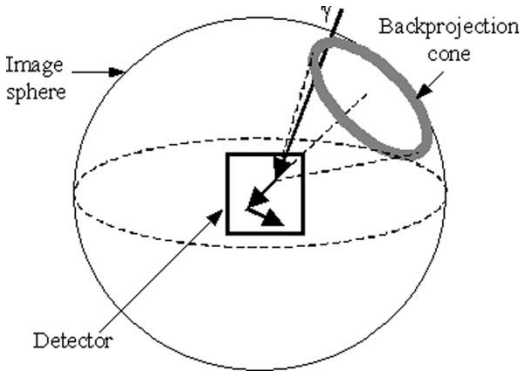


Fig. 1. Illustration of $4\pi$ Compton imaging. The backprojection cones are projected on a spherical image surface.

is possible to approximate the cone vertex to be at the center of the sphere. In this case, the intersection of the backprojected cone and the image sphere is simply a circle, and backprojection becomes extremely simple. For the $4\pi$ imager considered here, the far-field approximation is valid for source-detector distances greater than 20 cm, where error in the cone axis direction is less than $3^\circ$.

An important consideration in $4\pi$ imagers is directional sensitivity. To have uniform sensitivity to gamma rays from all directions would require spherical detectors, an unpractical geometry. In terms of uniform sensitivity, a cubic or even coaxial geometry would be more advantageous than a flat planar detector. The current detector is $15\ \mathrm{mm} \times 15\ \mathrm{mm} \times 10\ \mathrm{mm}$, which is not quite cubic. Thus, the sensitivity will be slightly lower for sources located beside the detector than for sources above or below it due to the smaller solid angle.

## III. Sequence Order Reconstruction

Before image reconstruction can be performed, the sequence of interactions must be decided. This is often called "tracking." In large traditional Compton imagers, timing can help determine the order of events. However, in the $4\pi$ imager the timing resolution of the detector is much larger than the flight time of a gamma ray between events, and thus timing cannot be used to determine the sequence order.

If only Compton scatter and photoelectric absorptions are assumed to occur (the probabilities for Rayleigh scatter and pair production are sufficiently low), the correct sequence can often be identified to high probability. The method for tracking used in the $4\pi$ Compton imager depends on the number of observed interactions.

### A. Two Interactions

For two interactions in the detector, the simplest and most popular method for determining the sequence of interactions is based on the energies deposited. A Geant4 simulation was performed in which monoenergetic gamma rays were incident on a 2.25-$\mathrm{cm}^3$ CdZnTe detector. The fraction of two-event sequences in which the first interaction deposits more energy than the second interaction was tallied for initial photon energies from 100 keV to 2 MeV, and the results are shown in Fig. 2. For

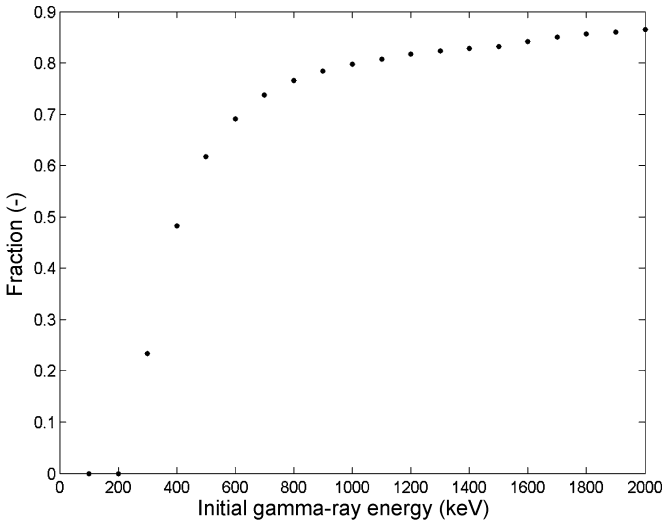


Fig. 2. Fraction of simulated two-event sequences in which the first interaction deposits more energy than the second interaction.

gamma-ray energies above 400 keV incident on CdZnTe, on average the first interaction deposited more energy. The reverse is true below 400 keV. Thus, a simple selection technique for two events consists of summing the two energies; then if the total is above (below) 400 keV, the interaction that deposits more (less) energy is designated the first event.

Fig. 2 also gives a measure of the success rate of this tracking scheme. At 662 keV, about 70% of sequences will be correctly identified. At 2 MeV, that fraction increases to over 85%. Note that below 256 keV, the scatter and absorption energy distributions are distinct and the first event always deposits less energy than the second.

### B. Three Interactions

When there are three interactions in the detector, the sequencing technique becomes more complicated. Typically, all six possible sequences are tested. Tracks that are not kinematically possible are discarded. The remaining sequences are assigned a figure of merit, for which the optimum value is chosen to determine the correct sequence. There are currently three techniques found in the literature for determining the sequence of three interactions.

One method for sequencing three events is called "backtracking" [6]. This method is based on the fact that the distribution of energies deposited in the photoelectric absorptions is roughly independent of the initial gamma-ray energy, given that more than one interaction occurs. Thus, an energy between 100 and 250 keV is assigned to the photoelectric interaction, and the gamma-ray track is reconstructed from last to first using the probabilities for photoelectric absorption and Compton scatter along with the Compton scatter formula. We did not attempt to implement backtracking with the $4\pi$ Compton imager.

Another method to sequence three events was proposed in [1]. Three-Compton reconstruction is combined with Compton kinematic discrimination to determine which of the six possible sequence orders is nonphysical. Then, a figure-of-merit is assigned to the physically realizable sequence orders using

the probability of observing the given sequence, calculated via the Klein-Nishina differential cross section for Compton scatter. The track with the largest figure-of-merit is then chosen. Simulations were performed to test this method with the $4\pi$ Compton imager. Only 40% of all sequences and 35% of full-energy sequences for 662 keV photons were correctly reconstructed. At 2.5 MeV, these fractions increased to 50% and 42%, respectively. The poor position resolution compared with the average distance between interactions (only 3 mm) is the major contributor to the poor reconstruction performance.

The so-called "chi-squared" method and its variants [7]–[10] compare the second scatter angle cosines calculated using the energies and positions independently. The figure-of-merit for this method is the square of the difference in cosines divided by the uncertainty in that difference. The track with the smallest figure-of-merit is chosen. (Some authors divide this FOM by the number of degrees of freedom, but since the minimum FOM is chosen this constant factor can be ignored.) This is not an exact chi-squared test in the statistical sense. For this reason we will refer to this method instead as the "minimum squared difference" (MSD) method. This method has been shown to be superior to the backprojection method in cylindrical Ge detectors [10]. In the $4\pi$ Compton imager, 57% of all sequences and 63% of full-energy sequences were correctly identified for 662 keV photons. At 2.5 MeV, 55% of all sequences and 72% of full-energy sequences were correctly identified. Because the method assumes that the entire gamma-ray energy is deposited, the sequence orders of full-energy tracks have a higher probability of being correctly determined. The MSD method is used throughout the remainder of this work.

### C. More Than Three Interactions

Determining the sequence order for more than three events is similar to that for three events. The above methods are used for every triplet of events in the sequence (for example, in sequence A-B-C-D, the triplets are A-B-C and B-C-D). Because the system is overdetermined, each triplet should be consistent with its adjacent triplets in terms of the scattered gamma-ray energies. Thus, the gamma-ray energy between points B-C should be the same for both A-B-C and B-C-D. This provides an additional constraint on the possible sequences. The figure-of-merit for physically realizable sequences is then calculated by summing the figures-of-merit for each triplet. The MSD method is used in this work to reconstruct sequences with four or more events.

## IV. Weighted List-Mode Maximum Likelihood

Simple backprojection implemented as described above can lead to poor images. As a result, iterative algorithms have been developed for reconstructing Compton images. The most popular iterative method for Compton imaging is maximum likelihood estimation [4], [5], [11]–[13].

Maximum likelihood methods are applied to $4\pi$ imaging in the same manner as traditional Compton imaging. MLEM attempts to reconstruct the source distribution with the highest likelihood of having produced the observed data. In practice, the MLEM reconstruction algorithm consists of a single update equation [5]

$$\lambda_j^{n+1} = \frac{\lambda_j^n}{S_j} \sum_i \frac{Y_i t_{ij}}{\sum_k t_{ik} \lambda_k} \tag{2}$$

where $\lambda_j^n$ is the estimated value of source pixel $j$ after $n$ iterations, $s_j$ is the probability that an emission from source pixel $j$ is observed anywhere in the detector, $Y_i$ is the number of times measurement $i$ is observed, $\boldsymbol{i} = \{1, 2, \ldots, i, \ldots, I-1, I\}$ includes all possible measurements, and $t_{ij}$ is the probability of observing measurement $i$ given an emission from source pixel $j$. The matrix $t_{ij}$ is also known as the system model or matrix. Using this equation, iterations are performed until either the maximum likelihood is achieved (and the image converges) or the iterations are terminated based on a designated stopping criterion.

As several authors have discussed [5], [11], [13], the number of elements required in the system matrix must be very large to minimize the information loss during reconstruction. Thus, list-mode maximum likelihood [13] was introduced to circumvent the binning of observed measurement data into $Y_i$. In the list-mode case, each measurement is taken individually, $i$ includes only measured events and $Y_i \rightarrow 1$ for all $i$. A value for $t_{ij}$ that can be calculated on the fly is advantageous and preferable to a system matrix that bins the data (resulting in lost information) and requires dedicated memory or a table look-up (resulting in lengthy reconstruction times).

Wilderman *et al.* [14] have proposed an analytical system model for list-mode maximum likelihood of Compton scatter images. The probability of observing a given measurement $A_i = \{E_0, E', r_{01}, r_{12}\}$ given a gamma ray incident from pixel $j$ is then

$$t_{ij} = \exp\left(-\sigma_t(E_0) r_{01}\right) \frac{d\sigma_C}{d\Omega} \exp\left(-\sigma_t(E') r_{12}\right) \tag{3}$$

where $\sigma_t(E)$ is the total absorption cross section at energy $E$, $E_0$ and $E'$ are the initial and scattered gamma-ray energies, respectively, $r_{01}$ is the attenuation distance between the source pixel and the first interaction, $r_{12}$ is the attenuation distance between the first and second interactions, and $d\sigma_C/d\Omega$ is differential Compton cross section, which is approximated by the Klein-Nishina cross section divided by $r_{12}^2$. Thus, the system model is the product of the probabilities of survival of the initial gamma ray to the first interaction point, scatter at the observed angle $\theta$, and survival of the scattered gamma ray to the second interaction location. The Klein-Nishina cross section is given below [15], where $\alpha = E_0/m_e c^2$ is the ratio of the initial gamma-ray energy to the rest mass energy of an electron

$$\frac{d\sigma_C}{d\Omega} \propto \left[\frac{1}{1+\alpha(1-\cos\theta)}\right]^2 \left(\frac{1+\cos^2\theta}{2}\right) \times \left[1 + \frac{\alpha^2(1-\cos\theta)^2}{(1+\cos^2\theta)\left[1+\alpha(1-\cos\theta)\right]}\right]. \tag{4}$$

In the above calculation, $\theta$ is the angle of scatter that would be observed if the gamma ray were incident from pixel $j$ and

interacted at the measured locations $r_1$ and $r_2$. In the calculation of the cross section in this paper , the initial gamma-ray energy is assumed to be the total energy deposited.

Due to the exponential terms in (3), higher probabilities are assigned to measurements in which the interaction distances are small. Furthermore, image pixels that lead to smaller apparent Compton angles, where the cross section peaks for medium and high-energy gamma rays, are also assigned a higher probability. Thus, although the product $\lambda_j t_{ij}$ is the forward projection and should produce the measurements most likely to be observed, the most likely measurements are also those with the largest uncertainties. Small distances between interactions result in very large geometric uncertainties. Forward scattered gamma rays lose a small fraction of their energies, leading to large (relative) energy uncertainties as well. Thus, the reconstructed angular uncertainties for the most likely sequences will be large. Ideally, the sequences leading to high angular uncertainty should be weighted less than those that lead to low uncertainty. A more accurate knowledge of the source location should be possible through such weighting.

Using $Y_i$ to weight sequences appropriately seems an obvious choice. Setting the $Y_i$ to the inverse of the estimated angular uncertainties $\Delta\theta_i$ will properly weight the sequences

$$Y_i = \frac{1}{\Delta\theta_i}. \tag{5}$$

Due to the finite position and energy resolution in the detector, the estimated angular resolution has a minimum positive value and therefore (5) will not result in infinite weighting.

The image must then be normalized to preserve absolute intensity information and the update equation becomes

$$\lambda_j^{n+1} = \frac{N\lambda_j^n}{S_j \sum_{i=1}^{N} (\Delta\theta_i)^{-1}} \sum_{i=1}^{N} \frac{(\Delta\theta_i)^{-1} t_{ij}}{\sum_{k=1}^{M} t_{ij}\lambda_k^n}. \tag{6}$$

The changes in the update equation should not affect the convergence of the iterations. Certainly, weighting each sequence with its angular uncertainty is no different than actually observing a higher number of low uncertainty data, and convergence does not depend on the observed data. The normalization factor is a constant for each iteration and also should not affect convergence. The positivity constraint is still automatically met.

To perform the reconstruction, we follow the method in [5] and first perform a backprojection for each sequence of interactions. Then, the calculation of the system matrix is carried out only for those pixels that intersect the backprojection cone. The width of the backprojection cone is given by $2\Delta\theta_i$.

Simulated data for 662 keV photons were reconstructed using both the traditional and weighted MLEM reconstruction methods. The FWHM of the central slice through the image was determined for each image as a function of the number of iterations performed. As shown in Fig. 3, the weighted MLEM method converges faster than the traditional MLEM method. In this work, no formal stopping criterion is used to determine the proper number of iterations, and ten iterations is chosen for all measured data to produce good results in a reasonable amount of time. On a personal computer with a 1.1-GHz Pentium III processor, the MLEM reconstruction speed was approximately 10 events per second per iteration.

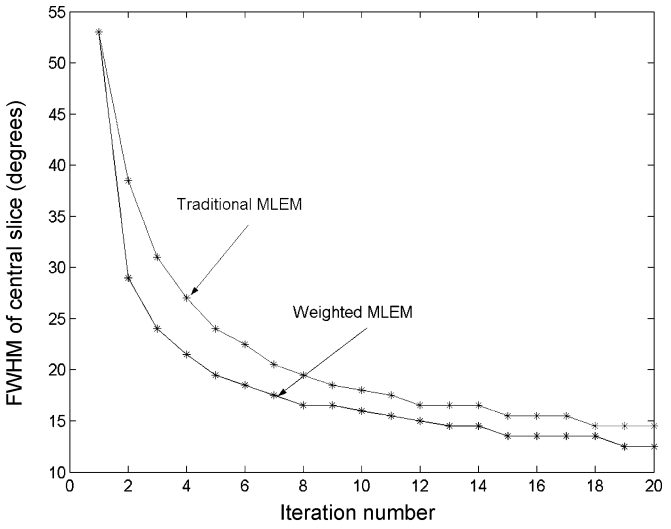


Fig. 3. FWHM of the central slice of the image as a function of iteration number of simulated 662 keV source reconstructed using WMLEM.

## V. Estimating Angular Uncertainty

The angular uncertainty of each sequence must be calculated for the sequence reconstruction, backprojection, and weighted MLEM steps. The uncertainties in the calculation of the first scatter angle and in the determination of the axis direction contribute to the total angular uncertainty for a given sequence. The scatter angle is calculated from measured energies, and the axis direction is calculated from measured positions. Thus, the uncertainties are independent and can be summed in quadrature to yield the total angular uncertainty.

The energy contribution is determined by carrying out a propagation of error analysis on the Compton scatter formula given in (1). Doppler effects are ignored in the estimation of angular uncertainty because the effect is small compared with the angular resolution achieved on this detector. The uncertainty $\Delta\theta_e$ in calculated Compton angle for $N$ total interactions in the sequence is then given by [see (7) at the bottom of the page] where $\Delta E_i$ is the estimated uncertainty in the energy deposited in the $i^{\text{th}}$ interaction.

Inherent in this calculation is the assumption that the initial gamma-ray energy is unknown but can be calculated by

$$\left(\frac{\Delta\theta_e}{m_e c^2}\right)^2 = \frac{(E_0 - E_1)^4 (\Delta E_1)^2 + \left[E_1^2 + 2E_1(E_0 - E_1)\right]^2 \left(\sum_{i=2}^{N} (\Delta E_i)^2\right)}{E_0^4 (E_0 - E_1)^4 \sin^2\theta} \tag{7}$$

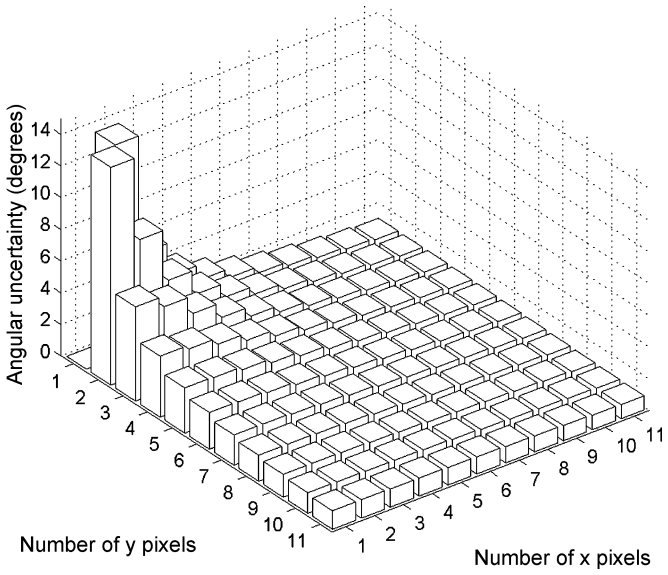


Fig. 4. Angular uncertainties due to geometry for two events occurring at the same depth separated by the given number of $x$ and $y$ pixels.

summing the $N$ deposited energies. Equation (7) would not apply in the cases where $E_0$ either is known a priori, such as in medical imaging applications, or is determined by a different method, such as in three-Compton reconstruction. (In fact, for three-Compton reconstruction, the positions and energies are both used to calculate the initial gamma-ray energy, and thus the uncertainties in cone axis and Compton angle are no longer independent.)

The uncertainty in the reconstruction cone axis is due to the pixellation in the lateral coordinates and the uncertain depth coordinate, and it is estimated in the following manner. The two interactions are assumed to occur somewhere inside voxels with dimensions corresponding to the position uncertainties in x, y, and z. A point is randomly chosen inside each voxel and a vector is drawn between the points. The angular deviation of this vector from the line connecting the centers of the voxels can then be determined. For each possible pair of two interactions voxels, 10 000 points are randomly chosen within the voxel, and the angular deviation is calculated for each point. The average of this distribution is considered to be the geometric uncertainty $\Delta\theta_g$. This method takes into account the fact that more volume is located along the line connecting the voxel centers than near the corners of the voxels, where the angular deviation is large. For the case where two interactions occur in neighboring pixels at the same depth, the calculated geometric uncertainty is only 15°, although the maximum angular deviation is nearly 90°. The geometric uncertainties for all possible interaction pairs at the same depth are given in Fig. 4.

Finally, the total angular uncertainty is simply the quadrature sum of the energy and position contributions:

$$\Delta\theta = \sqrt{\Delta\theta_e^2 + \Delta\theta_g^2}. \tag{8}$$

## VI. Performance of the $4\pi$ Compton Imager

The $4\pi$ Compton imager uses the 2.25-$\mathrm{cm}^3$ CdZnTe detector described in [3] operated under the following conditions. The cathode and steering grid electrode were biased at −2000 and −75 V, respectively, while the anode pixels were grounded. Six of the 121 anode pixels were not used due to poor performance. Sources were placed about 20 cm from the detector. Energy and position information was recorded during data acquisition for each sequence of interactions in the detector. Then, the measured data were used in list-mode to reconstruct images using the methods described previously. Only full-energy sequences were imaged, but there was no discrimination based on the distance between interactions. Two-, three-, and four-pixel sequences were considered; sequences with more than four events were discarded. Both traditional and weighted list-mode MLEM were used to reconstruct the data. Ten iterations were performed for all images to reduce computation time.

Full $4\pi$ images can be represented in several ways. The image can be separated into hemispheres and plotted as a contour, for example, for the left and right views simultaneously. Alternatively, the images can be represented as a surface on a plane with the lateral and azimuthal angles on the horizontal axes and the intensity on the vertical axis. This planar image would "wrap around" a sphere to produce the true image. The latter method is used here for the purposes of publication. It should be noted that in planar view the image pixel size varies from large at the center to small at the top and bottom. A point source at zenith would reconstruct to a line at the top of the planar image, while a point source along a horizontal line with respect to the detector would reconstruct to a point.

To demonstrate the benefits of using weighted MLEM method, a comparison is made with the traditional list-mode MLEM for several source configurations. First, a single 10 $\mu$Ci $^{137}$Cs source is placed 20 cm from the detector. The resulting unweighted and weighted images are shown in Figs. 5 and 6, respectively. It is clear that the response of weighted MLEM method is much sharper than the response of the traditional method.

A slice of the weighted image through the central source region yields the function shown in Fig. 7. The estimated resolution of the device using this method is approximately 17°. To verify this resolution, two $^{137}$Cs sources were placed 18° apart at 20 cm from the detector. Each source is a 3-mm disk, which is point-like at 20 cm. The source activities were not equal. A slice of the image through the two sources is shown in Figs. 8 and 9 for the unweighted and weighted MLEM methods, respectively. The image generated using the traditional method is again inferior. Two peaks are clearly visible in the weighted image while in the unweighted image the sources cannot be distinguished.

The concept of imaging efficiency for this detector is not straightforward. Typically, the intrinsic efficiency is defined as the fraction of incident gamma rays that contribute to the image. In the case of the $4\pi$ Compton imager, some sequences result in an incorrect backprojection cone due to charge sharing between pixels, multiple events occurring under a single pixel, incorrect event sequencing, etc.; these sequences are still imaged. In reality it is impossible to determine if the correct sequence order was chosen, if the gamma ray interacted more than once under one pixel, or if charge sharing occurred. If the gamma-ray energy is known, all that can be determined absolutely is that the total energy was deposited in the observed events, no pair pro-

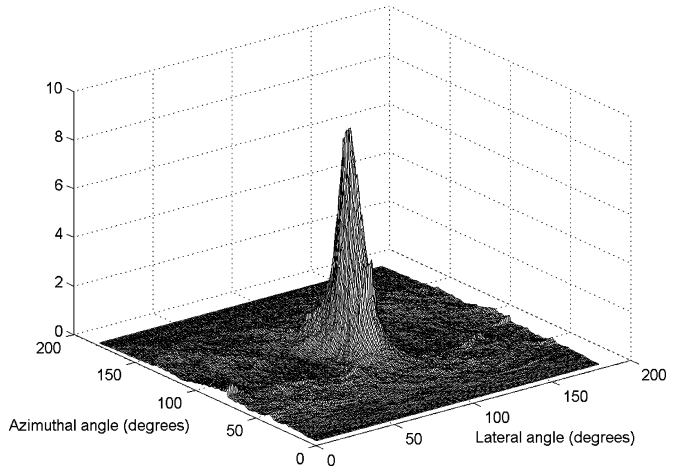


Fig. 5. Image of single $^{137}$Cs source at 20 cm using traditional list-mode MLEM reconstruction.

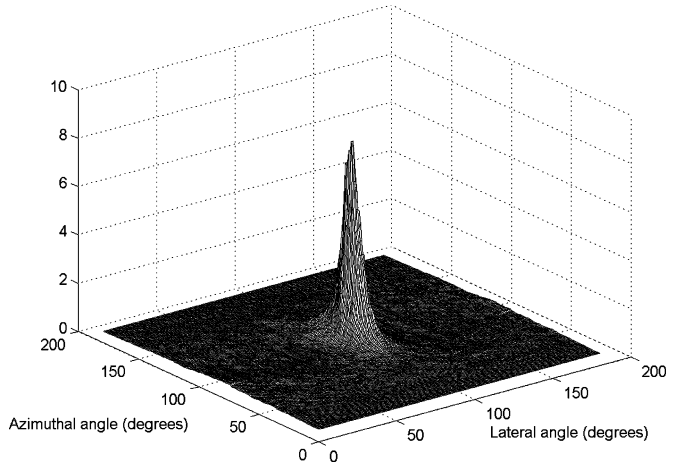


Fig. 6. Image of single $^{137}$Cs source at 20 cm using weighted list-mode MLEM reconstruction.

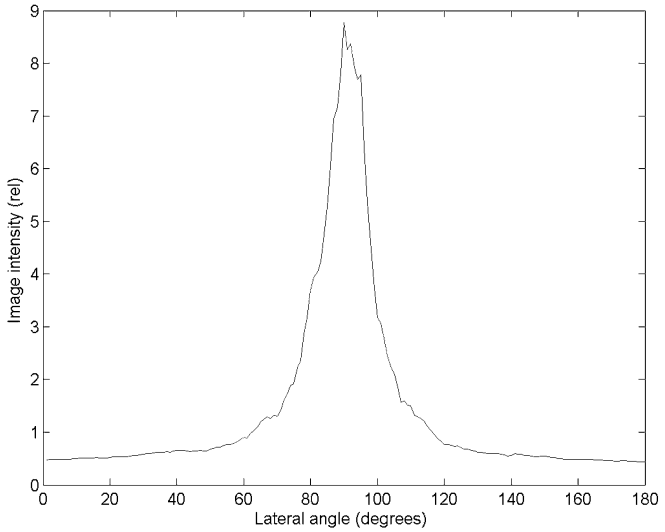


Fig. 7. Azimuthal slice of the image shown in Fig. 6. The FWHM of this distribution is 17°.

duction occurred, and the sequence is kinematically possible. Thus, the intrinsic imaging efficiency must be defined as the fraction of incident gamma rays that satisfy those three criteria.

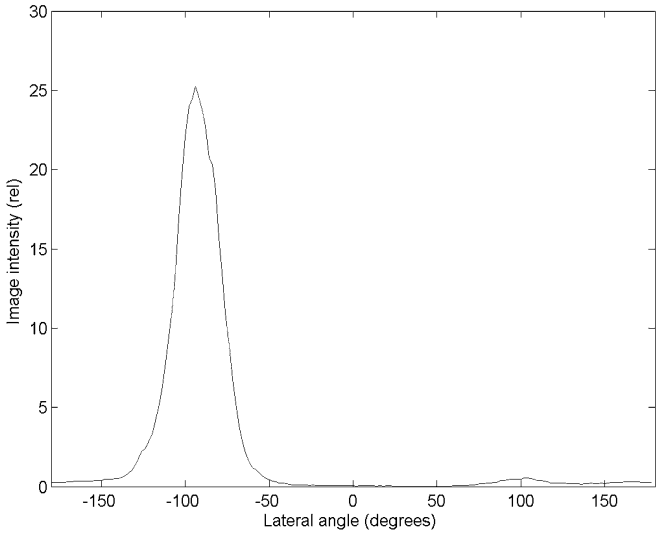


Fig. 8. Lateral slice of the image of two $^{137}$Cs sources separated by 18° using traditional list-mode MLEM reconstruction.

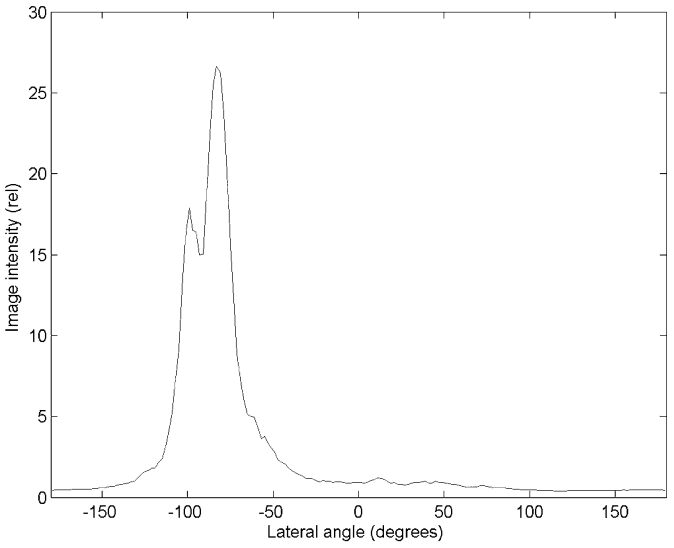


Fig. 9. Lateral slice of the image of two $^{137}$Cs sources separated by 18° using weighted list-mode MLEM reconstruction.

In this detector, 47% of measured full-energy sequences at 662 keV involve only one event; these sequences cannot be used for Compton imaging. Of the measured full-energy multiple-pixel sequences, nearly 74% satisfied the imaging criteria. The measured intrinsic imaging efficiency for 662 keV gamma rays was 1.9%. This is large, considering the size of the $4\pi$ Compton imager, and is three orders of magnitude higher than the previous two-detector prototype system [16].

## VII. Summary

We have demonstrated the use of a single three-dimensional (3-D) position-sensitive CdZnTe spectrometer as a $4\pi$ Compton imager. The imaging resolution of the device is improved using a weighted list-mode maximum likelihood image reconstruction method whereby each sequence is weighted by its estimated angular uncertainty. The weighted method preserves the

traditional MLEM assets: convergence, positivity, and conservation of counts. Using the current 2.25-$\mathrm{cm}^3$ CdZnTe detector we achieve an imaging resolution of 17° and an intrinsic imaging efficiency of nearly 2% at 662 keV.

## REFERENCES


[1] R. A. Kroeger, W. N. Johnson, J. D. Kurfess, B. F. Phlips, and E. A. Wulf, "Three-Compton telescope: theory, simulations, and performance," *IEEE Trans. Nucl. Sci.*, vol. 49, pp. 1887–1892, 2002.

[2] G. J. Schmid, D. A. Beckedahl, J. E. Kammeraad, J. J. Blair, K. Vetter, and A. Kuhn, "Gamma-ray Compton camera imaging with a segmented HPGe," *Nucl. Instrum. Methods*, vol. A459, pp. 565–576, 2001.

[3] F. Zhang, Z. He, G. F. Knoll, D. K. Wehe, J. E. Berry, and D. Xu, "Improved resolution for 3-D position-sensitive CdZnTe spectrometers," in *13th Int. Workshop on Room-Temperature Semiconductor X- and Gamma-Ray Detectors, IEEE Nuclear Science Symp.*, Portland, OR, 2003.

[4] A. P. Dempster, N. M. Laird, and D. B. Rubin, "Maximum likelihood from incomplete data via the EM algorithm," *J. Royal Statist. Soc.*, vol. B39, pp. 1–38, 1977.

[5] S. J. Wilderman, N. H. Clinthorne, J. A. Fessler, and W. L. Rogers, "List-mode likelihood reconstruction of Compton scatter camera images in nuclear medicine," in *Proc. IEEE Nuclear Science Symp. Conf. Rec.*, 2000, pp. 1716–1720.

[6] J. van der Marel and B. Cederwall, "Backtracking as a way to reconstruct Compton scattered gamma-rays," *Nucl. Instrum. Methods*, vol. A437, pp. 538–551, 1999.

[7] G. J. Schmid, I. Y. Lee, M. A. Deleplanque, P. Hendriks, F. S. Stephens, K. Vetter, S. J. Asztalow, R. M. Clark, R. M. Diamond, P. Fallon, R. Kruecken, A. O. Macchiavelli, and R. W. MacLeod, "Gamma-ray cluster identification in a spherical shell of highly segmented germanium detectors," *IEEE Trans. Nucl. Sci.*, vol. 44, pp. 975–978, 1997.

[8] I. Y. Lee, "Gamma-ray tracking detectors," *Nucl. Instrum. Methods*, vol. A422, pp. 195–200, 1999.

[9] U. G. Oberlack, E. Aprile, A. Curioni, V. Egorov, and K. L. Giboni, "Compton scattering sequence reconstruction algorithm for the liquid xenon gamma-ray imaging telescope (LXeGRIT)," in *SPIE Proc.*, vol. 4141, 2000, pp. 168–177.

[10] O. Wieland, F. Camera, B. Million, A. Bracco, and J. van der Marel, "Pulse distributions and tracking in segmented detectors," *Nucl. Instrum. Methods*, vol. A487, pp. 441–449, 2002.

[11] L. Parra and H. H. Barrett, "List-mode likelihood: EM algorithm and image quality estimation demonstrated on 2-D PET," *IEEE Trans. Nucl. Sci.*, vol. 17, pp. 228–235, 1998.

[12] L. A. Shepp and Y. Vardi, "Maximum likelihood reconstruction for emission tomography," *IEEE Trans. Nucl. Sci.*, vol. 1, pp. 113–122, 1982.

[13] H. H. Barrett, T. White, and L. C. Parra, "List-mode likelihood," *J. Opt. Soc. Amer.*, vol. A14, pp. 2914–2923, 1997.

[14] S. J. Wilderman, J. A. Fessler, N. H. Clinthorne, J. W. LeBlanc, and W. L. Rogers, "Improved modeling of system response in list mode EM reconstruction of Compton scatter camera images," *IEEE Trans. Nucl. Sci.*, vol. 48, pp. 111–115, 2001.

[15] G. F. Knoll, *Radiation Detection and Measurement*, 3rd ed. New York: Wiley, 2000.

[16] Y. Du, Z. He, G. F. Knoll, D. K. Wehe, and W. Li, "Evaluation of a Compton scattering camera using 3-D position sensitive CdZnTe detectors," *Nucl. Instrum. Methods*, vol. A457, pp. 203–211, 2001.